

# Upsilon Decays at CLEO

Steven Blusk

Syracuse University, Syracuse, NY 13244

Using data collected using the CLEO III detector, we present recent results on decays of the  $\Upsilon(1S) - \Upsilon(3S)$  resonances. We report on three analyses. They are: (1) improved measurements of the muonic branching fraction of the  $\Upsilon(1S) - \Upsilon(3S)$ , (2) precision measurements of  $\Upsilon(2S)$  and  $\Upsilon(3S)$  photonic transitions, and (3) new measurements of  $\Upsilon(1S)$  decays to charmonium final states.

## I. INTRODUCTION

Since their discovery in 1977, the  $\Upsilon$  resonances have provided a unique laboratory for the study of strong interactions (QCD), while the  $\Upsilon(4S)$  resonance provides a clean source of  $B$  mesons which are used to probe the weak interaction. The analyses reported on here make use of approximately  $20 \times 10^6$   $\Upsilon(1S)$ ,  $9 \times 10^6$   $\Upsilon(2S)$ , and  $5 \times 10^6$   $\Upsilon(3S)$  decays recorded using the CLEO III detector at CESR. The analyses also utilize  $0.2 \text{ fb}^{-1}$ ,  $0.4 \text{ fb}^{-1}$  and  $0.2 \text{ fb}^{-1}$  of data taken just below the  $\Upsilon(1S)$ ,  $\Upsilon(2S)$ , and  $\Upsilon(3S)$  resonances (*ie.*, *continuum*), respectively.

## II. MEASUREMENT OF THE MUONIC BRANCHING FRACTION IN $\Upsilon(1S)$ , $\Upsilon(2S)$ AND $\Upsilon(3S)$ DECAYS

The  $\Upsilon$  resonances have provided a fertile testing ground for both lattice QCD and QCD-inspired potential models. Of particular interest are the total widths of these resonances,  $\Gamma$ , which can be related to the muonic branching fraction,  $\mathcal{B}_{\mu\mu}$  via  $\Gamma = \Gamma_{ee}/\mathcal{B}_{\mu\mu}$ , where the electronic decay width,  $\Gamma_{ee}$ , can be obtained from the integrated resonant cross-section for  $e^+e^- \rightarrow \text{hadrons}$ .  $\mathcal{B}_{\mu\mu}$  also enters into the determination of other  $\Upsilon$  branching fraction measurements, and therefore may present a limiting systematic uncertainty. CLEO is now in a position to provide a much improved measurement of  $\mathcal{B}_{\mu\mu}$  [1].

The branching fraction  $\mathcal{B}_{\mu\mu}$  can be extracted by measuring the efficiency-corrected ratio:  $\tilde{\mathcal{B}} = N_{\Upsilon(1S) \rightarrow \mu^+\mu^-} / N_{\Upsilon(1S) \rightarrow \text{hadrons}}$ , which is related to  $\mathcal{B}_{\mu\mu}$  through  $\mathcal{B}_{\mu\mu} = \tilde{\mathcal{B}} / (1 + \tilde{\mathcal{B}})$ . Dimuon events are selected by requiring exactly two nearly back-to-back charged tracks ( $N_{trk}$ ) with energy  $E_\mu$  in the range  $0.7 < E_\mu/E_{beam} < 1.15$ , one which must be detected in the muon system. Hadronic events are selected by requiring  $N_{trk} \geq 3$ , with additional requirements on the energy in the calorimeter when  $N_{trk} < 5$ . The number of dimuon (hadronic) events surviving all analysis requirements are  $344.9 \times 10^3$  ( $18.96 \times 10^6$ ),  $119.6 \times 10^3$  ( $7.84 \times 10^6$ ), and  $81 \times 10^3$  ( $4.64 \times 10^6$ ) for  $\Upsilon(1S)$ ,  $\Upsilon(2S)$ , and  $\Upsilon(3S)$ , respectively. Event selection and analysis requirement efficiencies are determined from simulation and are 65% (96-98%) for the dimuon (hadronic) event selection. Backgrounds are estimated using simulation and are below 3% for

the dimuon samples and less than 1% for the hadronic samples. The branching fractions are found to be:  $\mathcal{B}(\Upsilon(1S) \rightarrow \mu^+\mu^-) = (2.49 \pm 0.02 \pm 0.07)\%$ ,  $\mathcal{B}(\Upsilon(2S) \rightarrow \mu^+\mu^-) = (2.03 \pm 0.03 \pm 0.08)\%$  and  $\mathcal{B}(\Upsilon(3S) \rightarrow \mu^+\mu^-) = (2.39 \pm 0.07 \pm 0.10)\%$ , where the first uncertainty is statistical and the second systematic. The  $\Upsilon(1S)$  measurement is consistent with previous measurements, but the  $\Upsilon(2S)$  and  $\Upsilon(3S)$  are larger by 2-3 standard deviations. These latter two measurements provide factor of 2-3 improvement in the precision to which these branching fractions are known while the  $\Upsilon(1S)$  result is by itself competitive with the world average.

## III. RADIATIVE DECAYS OF THE $\Upsilon(2S)$ AND $\Upsilon(3S)$

Measurements of the radiative decays of the  $\Upsilon$  resonances provide clues into the nature of the strong force and provides for unique tests of potential models and lattice QCD. For example, the electric dipole transition rate,  $\Gamma_{E1} = \mathcal{B}(\Upsilon(nS) \rightarrow \chi_{bJ}(n'P))\Gamma(nS)$  can be determined experimentally, and can in turn be used to extract the corresponding matrix element. The matrix elements and the mass splittings can be used to learn about the contributing spin-orbit and tensor interactions [3].

The events for this analysis [2] use the same hadronic event selection as in the  $\mathcal{B}_{\mu\mu}$  analysis. Radiative transitions are observed through their peaks in the inclusive photon energy spectrum. Photon candidates are required to be isolated from all charged particles and have a shower profile consistent with an electromagnetic shower. The predominant source of background arises from  $\pi^0 \rightarrow \gamma\gamma$  decay. Application of a  $\pi^0$  veto for low energy photons does not improve the signal significance due to accidental combinations where the signal photon and a random photon have an invariant mass near the  $\pi^0$  mass. Consequently, the  $\pi^0$  veto is not applied to the  $\Upsilon(3S) \rightarrow \chi_{bJ}(2P)$  and  $\Upsilon(2S) \rightarrow \chi_{bJ}(1P)$  analyses. On the other hand, a  $\pi^0$  veto is applied to the  $\Upsilon(3S) \rightarrow \chi_{bJ}(1P)$  analysis, where the photon energies are much higher and accidental combinatorial losses are much smaller.

The inclusive photon spectrum for  $\Upsilon(2S)$  data is shown in Fig. 1. The top figure shows the data (points) and overlaid are the fits to the data (solid line) and the

background contribution (dashed line). The lower plot shows the background subtracted peaks along with the fit (solid line) and the contributions from the individual  $\chi_{b,J}$  states (dashed line). The background is determined using a combination of continuum and  $\Upsilon(1S)$  data. The analogous distributions for  $\Upsilon(3S)$  data are shown in Fig. 2. In both cases, large signals are observed for each of the transitions. The yields, efficiencies, branching fractions and photon energies are summarized in Table I. The branching fraction measurements are by themselves about a factor of two better than the world average values. Using the inclusive photon spectrum, we also observe the rare transition,  $\Upsilon(3S) \rightarrow \chi_{b0}(1P)$ , which is found to have a branching fraction of  $0.30 \pm 0.04 \pm 0.10\%$ . This is the first measurement of this transition rate.

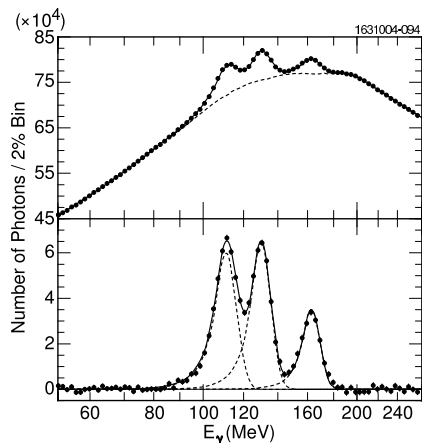


FIG. 1: Inclusive photon spectra in  $\Upsilon(2S)$  data (top) and the background subtracted spectrum (bottom). The solid line is the combined fit and the dashed line show the contributions from each of the  $\chi_{c,J}$  states.

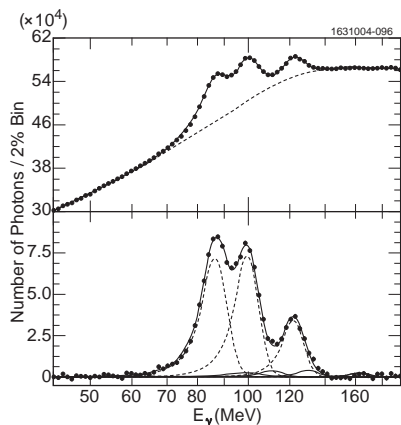


FIG. 2: Inclusive photon spectra in  $\Upsilon(3S)$  data (top) and the background subtracted spectrum (bottom). The solid line is the combined fit and the dashed line show the contributions from each of the  $\chi_{c,J}$  states.

#### IV. NEW MEASUREMENTS OF CHARMONIUM PRODUCTION IN $\Upsilon(1S)$ DECAY

One of the longstanding problems in QCD has been to understand the production mechanism for charmonium in a glue-rich environment. To account for the large excess of charmonium observed at the Tevtron, an additional color-octet mechanism [5] was proposed whereby a  $c\bar{c}$  pair is produced in a color-octet state, and then evolves non-perturbatively into a color-singlet. The matrix element for the latter was determined as to account for the deficit. It has been suggested that the study of  $J/\psi$  production in three-gluon decays of  $\Upsilon$  provides a unique opportunity to test color-octet predictions. The most dramatic expectation is a peaking of the  $J/\psi$  momentum spectrum near the kinematic endpoint. A second mechanism which can also produce  $J/\psi$  in  $\Upsilon$  decay is the color-singlet process,  $\Upsilon(1S) \rightarrow J/\psi c\bar{c}g + X$ , which is inherently soft and should yield two  $\psi$  additional open charm particles.

Events used in this analysis [4] are required to pass standard hadronic event selection. In order to suppress background from radiative return ( $e^+e^- \rightarrow \gamma J/\psi, \gamma\psi(2S)$ ), we reject events which have  $N_{trk} \leq 4$  and either a detected photon with momentum greater than 3.75 GeV/c, or an event momentum imbalance of larger than 2 GeV/c. Candidates  $J/\psi$ 's are reconstructed in the  $J/\psi \rightarrow \mu^+\mu^-$  and  $J/\psi \rightarrow e^+e^-$  modes. In addition to standard track selection criteria, muons are required to be detected in the muon system. Electrons are required to deposit energy in the calorimeter which is consistent with its measured momentum.

The invariant mass distributions for  $J/\psi \rightarrow \mu^+\mu^-$  and  $J/\psi \rightarrow e^+e^-$  candidates are shown in Fig. 3. The continuum contribution ( $e^+e^- \rightarrow J/\psi + X$ ) is estimated using data taken on and below the  $\Upsilon(4S)$ . This contribution is added to the expected  $\Upsilon(1S) \rightarrow \gamma^* \rightarrow q\bar{q} \rightarrow J/\psi + X$  contribution, and the total subtracted from the on- $\Upsilon(1S)$  data. The resulting scaled momentum distributions for  $J/\psi \rightarrow \mu^+\mu^-$  and  $J/\psi \rightarrow e^+e^-$  in  $\Upsilon(1S)$  decays are shown in Fig. 4. The data are compared to predictions of the color-octet (solid curve) and color-singlet (dashed curve). The data are much softer than the color-octet predictions and moderately softer than the color-singlet predictions. In the latter case, the effects of fragmentation of the recoiling charm into  $D, D^*, D^{**}, \Lambda_c$ , etc is not taken into account and is expected to further soften the spectrum. Integrating the spectrum, we measure a branching fraction  $\mathcal{B}(\Upsilon(1S) \rightarrow J/\psi + X) = (6.4 \pm 0.4 \pm 0.6) \times 10^{-4}$ . This measurement is consistent with predictions of both the color-octet and color-singlet models which predict branching fractions of  $6.2 \times 10^{-4}$  and  $5.9 \times 10^{-4}$ , respectively. We have also observed the first observation of the decay,  $\Upsilon(1S) \rightarrow \psi(2S) + X$  (see Fig. 5) and found evidence for  $\Upsilon(2S) \rightarrow \chi_{c,J} + X$ . The branching fractions are measured relative to  $\Upsilon(1S) \rightarrow J/\psi + X$ , and are found to be:  $\frac{\mathcal{B}(\Upsilon(1S) \rightarrow \psi(2S) + X)}{\mathcal{B}(\Upsilon(1S) \rightarrow J/\psi + X)} = 0.41 \pm 0.11 \pm 0.08$ ,

TABLE I: Summary of results on  $E1$  transitions in  $\Upsilon(2S \rightarrow \chi_{bJ}(1P))$  and  $\Upsilon(3S \rightarrow \chi_{bJ}(2P))$ . Where uncertainties are shown, the first is statistical and the second is systematic.

Process	$N_\gamma (\times 10^3)$	Eff. (%)	$\mathcal{B}$ (%)	$E_\gamma$ (MeV)
$\Upsilon(2S) \rightarrow \chi_{b0}(1P)$	$198 \pm 6$	57	$3.75 \pm 0.12 \pm 0.47$	$162.56 \pm 0.19 \pm 0.42$
$\rightarrow \chi_{b1}(1P)$	$407 \pm 7$	63	$6.93 \pm 0.12 \pm 0.41$	$129.58 \pm 0.09 \pm 0.29$
$\rightarrow \chi_{b2}(1P)$	$410 \pm 6$	61	$7.24 \pm 0.11 \pm 0.40$	$110.58 \pm 0.08 \pm 0.30$
$\Upsilon(3S) \rightarrow \chi_{b0}(2P)$	$225 \pm 7$	57	$6.77 \pm 0.20 \pm 0.65$	$121.55 \pm 0.16 \pm 0.46$
$\rightarrow \chi_{b1}(2P)$	$537 \pm 7$	63	$14.54 \pm 0.18 \pm 0.73$	$99.15 \pm 0.07 \pm 0.25$
$\rightarrow \chi_{b2}(2P)$	$568 \pm 6$	61	$15.79 \pm 0.17 \pm 0.73$	$86.04 \pm 0.06 \pm 0.27$

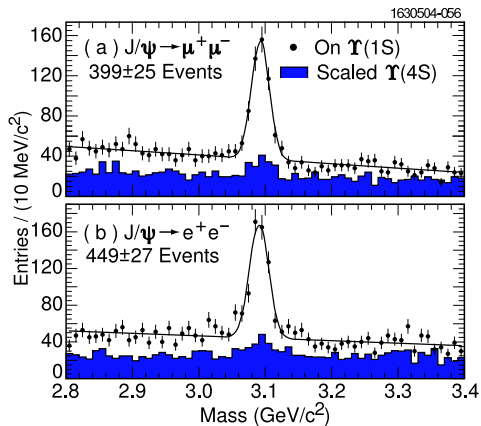


FIG. 3: Invariant mass distributions for  $\mu^+\mu^-$  and  $e^+e^-$  in  $\Upsilon(1S)$  data (points), and scaled  $\Upsilon(4S)$  continuum data (shaded).

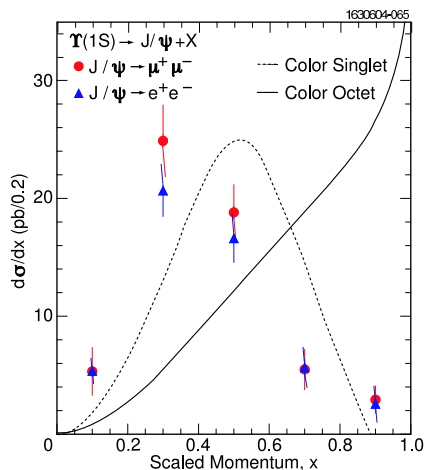


FIG. 4: Scaled momentum spectrum for  $\Upsilon(1S) \rightarrow J/\psi + X$  in three-gluon decays of the  $\Upsilon(1S)$  for  $J/\psi \rightarrow \mu^+\mu^-$  (circles) and  $J/\psi \rightarrow e^+e^-$  (triangles). The curves show the predictions of the color-octet and color-singlet models.

$\frac{\mathcal{B}(\Upsilon(1S) \rightarrow \chi_{c1} + X)}{\mathcal{B}(\Upsilon(1S) \rightarrow J/\psi + X)} = 0.35 \pm 0.08 \pm 0.06$ ,  $\frac{\mathcal{B}(\Upsilon(1S) \rightarrow \chi_{c2} + X)}{\mathcal{B}(\Upsilon(1S) \rightarrow J/\psi + X)} = 0.52 \pm 0.12 \pm 0.09$ , and  $\frac{\mathcal{B}(\Upsilon(1S) \rightarrow \chi_{c0} + X)}{\mathcal{B}(\Upsilon(1S) \rightarrow J/\psi + X)} < 7.4$  at 90% confidence level.

The feed-down contributions to  $J/\psi$  are about a factor of two higher than expected. These measurements have the potential to shed some additional light on the production mechanisms of charmonium in glue-rich environments.

I gratefully acknowledge the effort of the CESR staff in providing us with excellent luminosity and running conditions. I also thank the National Science Foundation and the U.S. Dept. of Energy for their support of this research.

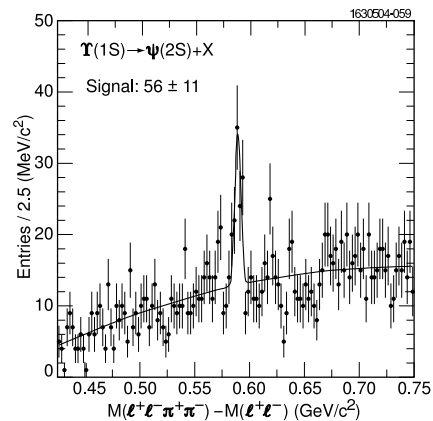


FIG. 5: Scaled momentum spectrum for  $\Upsilon(1S) \rightarrow J/\psi + X$  in three-gluon decays of the  $\Upsilon(1S)$  for  $J/\psi \rightarrow \mu^+\mu^-$  (circles) and  $J/\psi \rightarrow e^+e^-$  (triangles). The curves show the predictions of the color-octet and color-singlet models.

- [1] G. Adams *et al.*, [CLEO Collaboration] Submitted to Phys. Rev. Lett. [hep-ex/0409027].  
 [2] To be submitted to Phys. Rev. Lett.  
 [3] D. Besson and T. Skwarnicki, Annu. Rev. Nucl. Part. Sci

- 43**, 333 (1993).  
 [4] D. A. Briere *et al.*, [CLEO Collaboration] Accepted for publication in Phys. Rev. D [hep-ex/0407030].  
 [5] E. Braaten and S. Fleming, Phys. Rev. Lett. **74**, 3327

(1995) [hep-ph/9411365].